Viscoelastic effects on drop deformation in a converging pipe flow

Diwen Zhou

Department of Chemical and Biological Engineering, University of British Columbia, Vancouver, BC V6T 1Z3, Canada

Pengtao Yue and James J. Feng[a)]

Department of Chemical and Biological Engineering, and Department of Mathematics, University of British Columbia, Vancouver, BC V6T 1Z2, Canada

(Received 4 May 2007; final revision received 4 January 2008)

Synopsis

This paper reports finite-element simulations of drop deformation in converging flows in an axisymmetric conical geometry. The moving interface is captured using a diffuse-interface model and accurate interfacial resolution is ensured by adaptive refinement of the grid. We have explored the effects of viscoelasticity on drop deformation when either the drop or the matrix is a Giesekus fluid. Contrary to the popular belief that viscoelasticity in the drop hinders deformation and that in the matrix enhances deformation, we predict a more complex picture in which viscoelasticity in either component may suppress or promote drop deformation depending on the capillary number Ca and the drop-to-matrix viscosity ratio β. Smaller Ca and β are conducive to the behavior mentioned above, while large Ca and β may produce the opposite effect. Both trends are explained by the reaction of the polymer stress to the inhomogeneous and transient deformation in the converging flow field. Finally, this understanding reconciles contradictory results in the literature as opposite limits in the parameter space. © *2008 The Society of Rheology.*
[DOI: 10.1122/1.2837525]

I. INTRODUCTION

Drop deformation in a flowing medium is important to processing engineering materials such as emulsions and polymer blends [Tucker and Moldenaers (2002)] and to physiological processes in microcirculation [Zhou *et al.* (2007)]. In both contexts, the fluid components are often non-Newtonian complex fluids containing macromolecules, and the drop deformation depends on their viscoelastic rheology. In homogeneous shear and extensional flows, numerous studies have formed a rather coherent picture on how capillary, viscous and viscoelastic forces affect drop deformation [Rallison (1984); Stone (1994); Ramaswamy and Leal (1999a,1999b); Hooper *et al.* (2001b); Greco (2002); Yue *et al.* (2005b,2005c, 2006b); Sibillo *et al.* (2006); Khismatullin *et al.* (2006)]. In simple shear flows, viscoelasticity in the drop tends to reduce drop deformation while that in the matrix has a non-monotonic effect: it reduces drop deformation in lower Deborah number

[a)]Author to whom correspondence should be addressed; electronic mail: jfeng@chml.ubc.ca

but increases drop deformation with stronger viscoelasticity [Yue *et al.* (2005c)]. In uniform extensional flows, a polymer drop deforms less than its Newtonian counterpart while a polymer matrix tends to enhance drop deformation [Ramaswamy and Leal (1999a,1999b); Hooper *et al.* (2001b)]. This is consistent with the heuristic idea that drop deformation is controlled by the balance among fluid stresses inside and outside and the interfacial tension [Ghodgaonkar and Sundararaj (1996)].

In comparison, our knowledge of drop deformation in *inhomogeneous* flow geometries, such as channels or pipes with varying cross sections, is rather fragmentary and sometimes contradictory. In the conical section of a converging pipe flow, a drop moving along the centerline experiences inhomogeneous and time-dependent elongation. Of the handful of experiments in this geometry, Chin and Han (1979) reported that increasing the polymer concentration in the drop fluid suppresses drop deformation, while increasing the polymer concentration in the matrix has the opposite effect. This seems consistent with the behavior in homogeneous elongation. The more recent experiment of Bourry *et al.* (1999), on the other hand, was inconclusive as to whether a polymeric drop deforms more or less than a Newtonian one with comparable viscosity. Both experiments were complicated by the strong strain-rate-dependent rheology of the fluids; it is uncertain whether the effect is due to elasticity or viscosity that has changed with the deformation. As a matter of fact, Kim and Han (2001) later attributed the observations of Chin and Han (1979) entirely to viscosity. Mighri *et al.* (1997) attempted to clear up this issue by carrying out similar experiments with Boger fluids in one or both components. Their results seem in agreement with the simple argument advanced in homogeneous elongational flows: polymer in the drop hinders its deformation while that in the matrix enhances deformation. These authors further correlated drop deformation with the difference in elasticity between the drop and the matrix. In the only theoretical or computational study known to us, Khayat (1998) computed drop deformation in a conical pipe using a linear Oldroyd-B model. The results exhibit the opposite trend to that of Mighri *et al.* (1997). That is, a polymeric drop deforms more while a polymeric matrix causes a suspended drop to deform less.

This contradiction was the initial motivation for the present work. Using the nonlinear Giesekus model, we have systematically investigated the effect of viscoelasticity on drop deformation in a converging pipe flow over a wide range of the Deborah number. The results reveal an intricate picture that contains both prior studies as special cases at opposite ends of the parameter space. Note that historically, the conical geometry has been used as an *imperfect* device for generating elongational flows in which to measure the fluid's elongational viscosity [Cogswell (1972)] or to study drop deformation [Chin and Han (1979)]. Our perspective is different: we see this not only as a prototypical geometry for various polymer processing operations, but also as an inhomogeneous flow that is simple enough to allow detailed analysis of the fluid mechanics of drop deformation.

II. THEORETICAL MODEL AND NUMERICAL METHOD

To simulate a moving internal boundary, one either tracks it with boundary grids that are part of a moving mesh or captures it on a fixed grid using some scalar field [Sethian and Smereka (2003)]. In this work, we employ the diffuse-interface method in the latter category. In this model, the two nominally immiscible fluid components are assumed to mix in a thin interfacial region; a phase field ϕ varies smoothly from one bulk value ($\phi=-1$) to the other ($\phi=1$). The interfacial tension derives from a mixing energy that is a functional of ϕ. One advantage of this method is in handling morphological changes

such as drop coalescence [Yue *et al.* (2005a)]. But in the present problem, it is mostly a numerical device for capturing the deforming and moving drop surface. The diffuse-interface model has been the subject of several reviews [Anderson *et al.* (1998); Lowengrub and Truskinovsky (1998); Feng *et al.* (2005)], and the numerical implementation used here has also been detailed before [Yue *et al.* (2006b)]. Therefore, we will give only a brief outline in the following.

Through a formal variational procedure, one may derive the governing equations of a two-phase system consisting of a Newtonian fluid and a Giesekus fluid:

$$\nabla \cdot \boldsymbol{v} = 0, \tag{1}$$

$$\rho\left(\frac{\partial \boldsymbol{v}}{\partial t} + \boldsymbol{v} \cdot \nabla \boldsymbol{v}\right) = -\nabla p + \nabla \cdot \boldsymbol{\tau} + G\nabla\phi + \rho \boldsymbol{g}, \tag{2}$$

$$\boldsymbol{\tau} = \left(\frac{1-\phi}{2}\mu_n + \frac{1+\phi}{2}\mu_s\right)[\nabla \boldsymbol{v} + (\nabla \boldsymbol{v})^{\mathrm{T}}] + \frac{1+\phi}{2}\boldsymbol{\tau}_p, \tag{3}$$

$$\boldsymbol{\tau}_p + \lambda_H \boldsymbol{\tau}_{p(1)} + \alpha\frac{\lambda_H}{\mu_p}\boldsymbol{\tau}_p \cdot \boldsymbol{\tau}_p = \mu_p[\nabla \boldsymbol{v} + (\nabla \boldsymbol{v})^{\mathrm{T}}], \tag{4}$$

$$G = \lambda\left[-\nabla^2\phi + \frac{\phi(\phi^2-1)}{\epsilon^2}\right], \tag{5}$$

$$\frac{\partial \phi}{\partial t} + \boldsymbol{v} \cdot \nabla\phi = \gamma\nabla^2 G, \tag{6}$$

where $\rho = \frac{1-\phi}{2}\rho_1 + \frac{1+\phi}{2}\rho_2$ is the average density between the two fluids, G is the chemical potential derived from a Landau–Ginzburg mixing energy, μ_n is the viscosity of the Newtonian component, and μ_s and μ_p are the solvent and polymer viscosities of the Giesekus component. In the Giesekus model, λ_H is the polymer relaxation time, α is the so-called mobility factor, and the subscript (1) denotes upper convected derivative [Bird *et al.* (1987a)]. We have taken the Newtonian component to be fluid 1 ($\phi = -1$) and the Giesekus component fluid 2 ($\phi = 1$). In the simulations, either may be the drop or matrix fluid. The diffuse-interface model has three parameters: the mixing energy density λ, the capillary width ϵ and the molecular mobility γ. These are chosen so that the proper sharp-interface limit is approached [Jacqmin (1999); Liu and Shen (2003); Yue *et al.* (2007)], with the interfacial tension being $\sigma = \frac{2\sqrt{2}}{3}\frac{\lambda}{\epsilon}$.

The Giesekus model is used chiefly because it strikes a balance between simplicity and realistic rheological predictions. Derived from a dumbbell model with anisotropic viscous friction and Brownian motion [Bird *et al.* (1987b)], the Giesekus model is perhaps the simplest nonlinear model with reasonable normal stress differences. Applied to polymer melts and solutions in step shear, startup of uniaxial elongation and step biaxial extension, the Giesekus model "can describe the shear damping function and elongational viscosity quite accurately" [Khan and Larson (1987); Tirtaatmadja and Sridhar (1995)]. In prior computations on drop breakup and coalescence, the Oldroyd-B model sometimes caused difficulties in convergence [Yue *et al.* (2006a)]. Although this is not a concern for the relatively mild strain rates in this work, we nevertheless prefer the Giesekus model as it better represents the rheology of real polymeric liquids.

The computations are done in an axisymmetric geometry using AMPHI, a finite-element package based on the diffuse-interface model with adaptive meshing developed

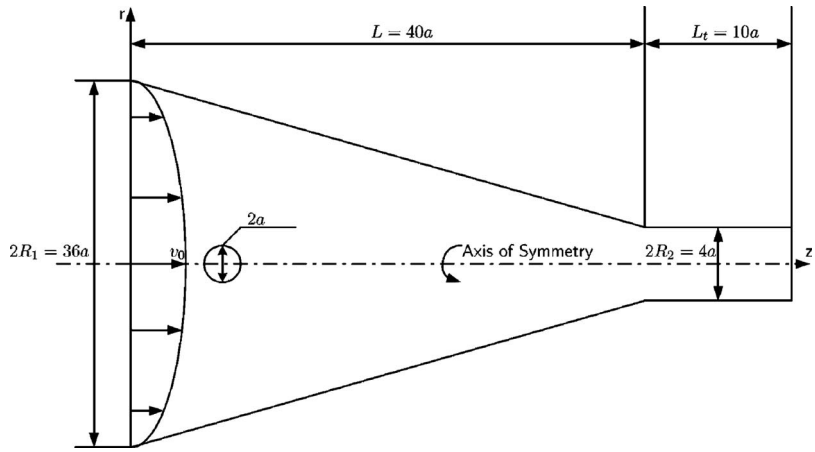

FIG. 1. Schematic of the flow geometry, with the computational domain being half of the meridian plane. Not drawn to scale.

for interfacial flows of complex fluids [Yue *et al.* (2006b)]. The governing equations are discretized using Galerkin finite elements on an unstructured triangular grid, with second-order fully implicit time stepping that requires Newton iteration at each time step. More details of the numerical method can be found in Yue *et al.* (2006a,2006b), who also reported detailed parametric studies and validation with benchmark problems. Adequate spatial and temporal resolution is ensured for the simulations presented in the following. Discretization errors are controlled to within 1% of the results.

III. PROBLEM SETUP

Figure 1 depicts the axisymmetric geometry of the converging flow channel. The computational domain is the upper half of the meridian plane. On the upstream boundary, we specify a parabolic profile for the axial velocity v_z with a centerline velocity v_0 and zero radial velocity v_r. If the matrix fluid is viscoelastic, we also impose fully developed polymer stresses at the entrance. Fully developed entrance conditions are not exactly correct in our geometry, even if it is preceded by a long straight section upstream. They are used here for simplicity, and numerical experiments show that the drop deformation in the conical section is not sensitive to the entry condition. For example, imposing the steady velocity and stress profiles at the beginning of the contraction that have been computed with a long straight section upstream will produce a 3% difference in drop deformation. Along the centerline, we assume conditions of symmetry with $\frac{\partial}{\partial r}=0$ for all velocity and stress components except $v_r=0$. At the exit, natural boundary conditions are used. Initially, a spherical drop of radius a is placed at $z_0=5a$ on the centerline in a quiescent matrix; the initial velocity and stress fields are zero. At time $t=0$, the inflow velocity profile is activated and the flow starts throughout the domain. The drop elongates while moving down the centerline of the pipe.

Upon non-dimensionalizing the governing equations and boundary conditions, the following six dimensionless groups emerge (in addition to the Giesekus mobility α and the four length ratios indicated in Fig. 1):

$$\omega = \frac{\rho_d}{\rho_m} \quad \text{(drop-to-matrix density ratio)}, \tag{7}$$

$$\beta = \frac{\mu_d}{\mu_m} \quad \text{(drop-to-matrix viscosity ratio)}, \tag{8}$$

$$k = \frac{\mu_s}{\mu_s + \mu_p} \quad \text{(solvent viscosity ratio in Giesekus fluid)}, \tag{9}$$

$$Ca = \frac{\mu_m a \bar{\dot{\epsilon}}}{\sigma} \quad \text{(capillary number)}, \tag{10}$$

$$Re = \frac{\rho_m v_0 a}{\mu_m} \quad \text{(Reynolds number)}, \tag{11}$$

$$De = \bar{\dot{\epsilon}} \lambda_H \quad \text{(Deborah number)}, \tag{12}$$

where the subscripts d and m denote the drop and matrix components. For the viscoelastic fluid, the total zero-shear viscosity $\mu_s + \mu_p$ is used in computing β, be it in the drop or the matrix. Since the strain rate varies along the centerline, we have used an averaged strain rate $\bar{\dot{\epsilon}}$ in defining the capillary and Deborah numbers. Assuming that the centerline velocity varies according to the inverse of the cross-sectional area, the total Hencky strain from $z=0$ to $z=L$ is $2 \ln \frac{R_1}{R_2}$ and the total transit time is

$$t_{tr} = \int_0^L \frac{dz}{v_z} = \frac{L}{3v_0} \frac{R_1^2 + R_1 R_2 + R_2^2}{R_1^2}. \tag{13}$$

We define the average strain rate $\bar{\dot{\epsilon}}$ as the ratio between these two quantities.

Several parameters are fixed throughout the simulations. The drop-to-matrix density ratio is kept at $\omega=1$, and the Reynolds number remains at $Re=0.01$ so inertia is negligible. All the length ratios are fixed at their values in Fig. 1. To avoid the stress blowup in the Oldroyd-B model but to produce sufficiently large viscoelastic stresses, we have used a small $\alpha=0.03$ for all the simulations. The polymer relaxation time is varied over a wide range to capture a comprehensive picture of the viscoelastic effect. Thus, the value of rheological parameters is based more on the need to reveal interesting physics than to approximate specific fluids. The discussion in the next section will focus on the effects of Ca, β, and De on drop deformation.

IV. NUMERICAL RESULTS

To explore the drop deformation in a converging pipe flow, we have done three groups of simulations: a Newtonian drop in a Newtonian matrix as the baseline, a Giesekus drop in a Newtonian matrix, and a Newtonian drop in a Giesekus matrix.

In the literature, drop deformation has been represented by two length ratios: $\frac{l-b}{l+b}$ and $\frac{l}{a}$, l and b being the half length and half breadth of the drop. The first is sensitive to small departures from sphericity, while the second is more suitable for highly elongated drops [Stone *et al.* (1986); Tretheway and Leal (2001)]. We will use $D=\frac{l}{a}$ in this paper since the drop deformation may be quite large.

When the rheology of either the drop or the matrix changes, the drop speed and displacement will vary. Thus, it is awkward to compare D based on the same time or the same drop position on the centerline. Following Mighri *et al.* (1997), we use the matrix strain *in the absence of the drop* as the benchmark for comparing drop deformation. From

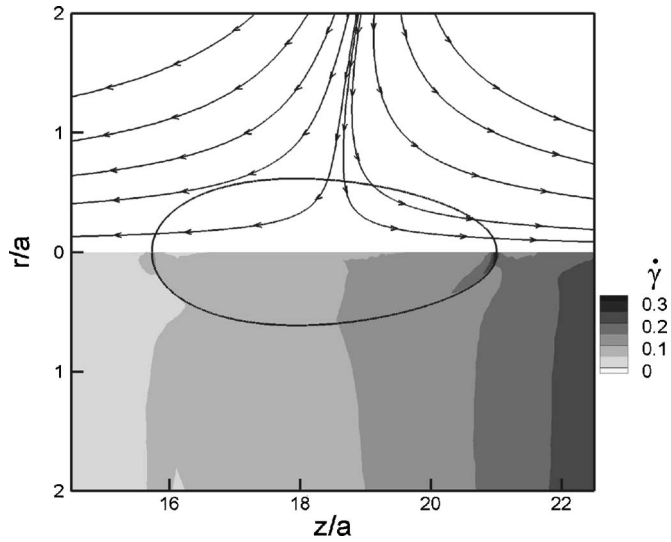

FIG. 2. A snapshot of the flow field around the drop when $D_m=2.5$ and the drop centroid is near $z=18a$. $Ca=2.9$, $\beta=0.5$. The top half shows streamlines in a reference frame fixed on the centroid of the drop, while the bottom half shows contours of the strain rate $\dot{\gamma}$, the second invariant of the strain rate tensor. For a clearer view of the drop interior, we have magnified the r coordinate relative to z.

the local strain rate $\dot{\epsilon}=\frac{dv_z}{dz}$ on the centerline, the matrix Hencky strain ϵ_m can be calculated. The corresponding matrix stretch ratio $D_m=\exp(\epsilon_m)$ turns out to be

$$D_m(z)=\frac{v_z(z)}{v_z(z_0)}, \tag{14}$$

where $z_0=5a$ is the initial position of the drop. Thus, $D_m(z)$ is the deformation of a matrix fluid particle currently at z with respect to its initial configuration at z_0, where the undeformed drop sits initially. Drop deformation D will be examined vis-à-vis the matrix deformation D_m at the same z as the drop's centroid on the centerline of the converging pipe.

A. A Newtonian drop in a Newtonian matrix

In our geometry, the drop experiences a spatially inhomogeneous and temporally transient extensional flow as it moves along the centerline of the converging pipe. Figure 2 depicts the kinematics of the flow around the drop. The streamlines, in a reference frame fixed on the centroid of the drop, resemble those of an elongational flow but exhibit a fore-aft asymmetry. Consequently, the drop is asymmetric as well, being more elongated in the front. The contours of the strain rate exhibit a general increase downstream. But within the drop, $\dot{\gamma}$ achieves a maximum at the front tip.

Figure 3 depicts the deformation of a Newtonian drop in a Newtonian matrix for several viscosity ratios. Comparing the $D(z)$ and $D_m(z)$ profiles in Fig. 3(a), we note that for the relatively high capillary number $Ca=2.9$, the drop deforms more than the matrix if it is less viscous ($\beta=0.01$) and vice versa ($\beta=2$), in agreement with experimental observations [Delaby *et al.* (1994)]. For D_m, we also plot a curve based on the exact Stokes flow solution in an infinite cone [van der Reijden-Stolk and Sara (1986)]. The actual stretching ratio turns out to be rather higher than the analytical solution, thanks to the inlet and outlet conditions.

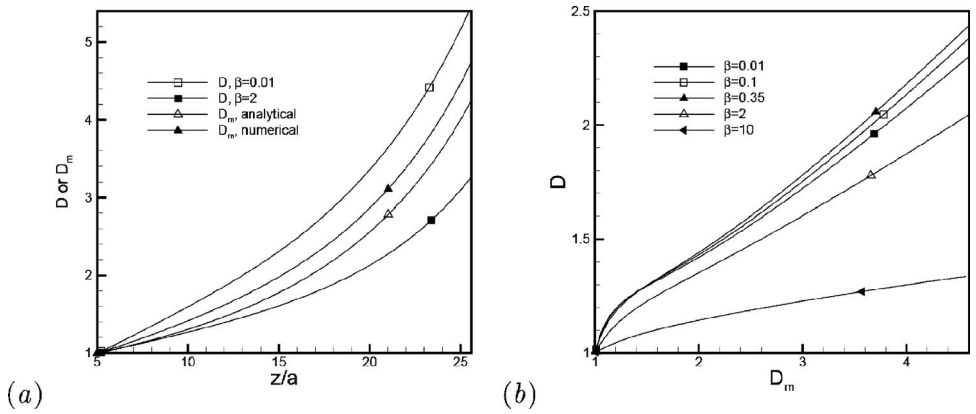

FIG. 3. (a) Drop and matrix deformation as functions of the position z for Newtonian systems at $Ca=2.9$. For the drop deformation D, two viscosity ratios are shown. For the matrix deformation D_m, an analytical result based on creeping flow in an infinite cone is also shown for comparison [van der Reijden-Stolk and Sara (1986)]. (b) Drop deformation D as a function of the matrix deformation D_m for Newtonian systems at $Ca=0.29$.

Figure 3(b) plots the drop deformation D as a function of the matrix deformation D_m for five β values. All curves have an initial transient, obviously due to the somewhat artificial initial condition, but eventually assume a constant slope. This linearity has been observed experimentally by Mighri *et al.* (1997). In steady and homogeneous elongation, the steady-state deformation of a drop (for subcritical Ca) is often viewed as the result of the balance between viscous and capillary forces. In our situation, the strain rate in the matrix continues to increase as the drop moves downstream [cf. Fig. 3(a)], as does the viscous force. Thus, the drop deformation increases continuously. For the rest of the paper, we will use the slope S of the straight portion of the $D(D_m)$ curves to indicate the speed of drop deformation. For Newtonian systems, S will be shown to depend on Ca and β, while for non-Newtonian fluids, the Deborah number De is involved as well.

A curious observation in Fig. 3(b) is that for this Ca the drop deformation does not seem to depend on the viscosity ratio β monotonically. This effect is more clearly illustrated in Fig. 4 in terms of the slope S. For smaller Ca, there is an intermediate viscosity ratio β_M at which the drop deforms the fastest. With Ca increasing from 0.29 to 1.45, β_M decreases from approximately 0.35–0.20, and seems to disappear for larger Ca.

The nonmonotonic dependence of S on β can be explained by the transient deformation of a drop after the startup of an elongational flow at a fixed strain rate. Numerical computations by Hooper *et al.* (2001b) show that a more viscous drop reacts to the startup more slowly; its initial deformation lags behind that of a less viscous drop. However, it eventually achieves a greater steady-state deformation, provided that Ca is below the critical value for drop burst. The slower initial reaction is due to a longer "emulsion time" $t_{em}=\frac{\mu_d a}{\sigma}$ for the drop [Sibillo *et al.* (2004)], and the greater steady-state deformation is because the more viscous interior sustains higher internal stresses so as to afford the exterior fluid a firmer "grip" on the interface. In our geometry, the drop experiences an unsteady external flow in the Lagrangian sense. So it deforms continually and is in a perpetual transient state. For small β values, t_{em} is short and the drop is close to equilibrating with the local strain rate. Thus, it exhibits the *steady-like* behavior with the instantaneous $D(t)$ increasing with β. For large β values, the contrary is true and the drop is dominated by the *transient* response, with $D(t)$ decreasing with β. This explains

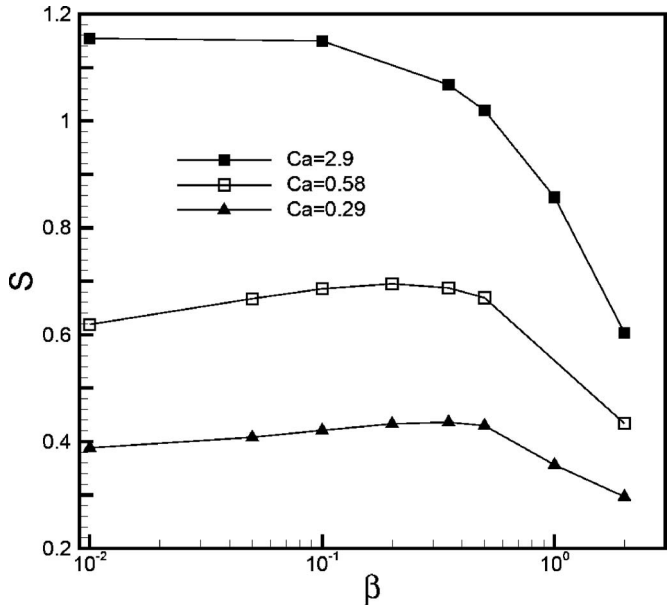

FIG. 4. The slope of drop deformation S as a function of viscosity ratio β in Newtonian systems at different Ca.

the non-monotonic $S(\beta)$ curves in Fig. 4 for smaller Ca. Larger Ca may be thought of as the result of increased flow rate or decreased interfacial tension. Either way, a drop would take longer dimensional time to reach steady state upon startup of the uniform elongation. In our geometry, therefore, the transient response prevails and D decreases with β monotonically. This monotonic decrease confirms previous computations in the limit of $Ca \to \infty$ [Bourry *et al.* (1999)].

B. A Giesekus drop in a Newtonian matrix

Figure 5 depicts the deformation of viscoelastic Giesekus drops as a function of the

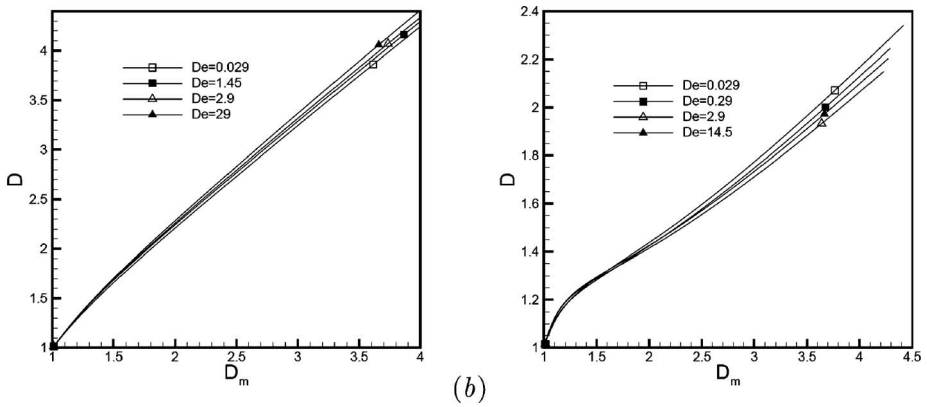

FIG. 5. Deformation of Giesekus drops as a function of the Newtonian matrix deformation with β=0.5 and k=0.2. (a) Ca=2.9; (b) Ca=0.29. Although the differences among the curves are small in magnitude, they are much greater than discretization errors and represent a real physical effect.

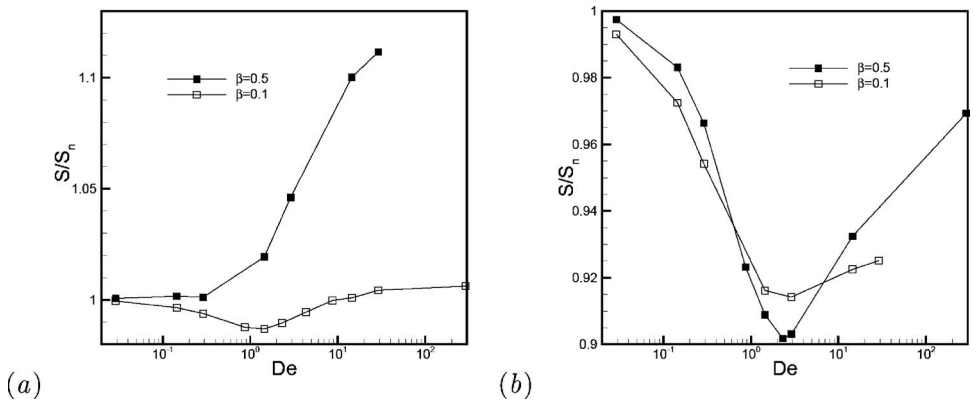

FIG. 6. Viscoelastic effects on the deformation of a Giesekus drop in a Newtonian matrix at (a) $Ca=2.9$, (b) $Ca=0.29$. The drop deformation is represented by the slope S scaled by the corresponding Newtonian slope S_n, and exhibits different trends with varying Deborah number De. For all cases, the Giesekus fluid has a solvent viscosity ratio $k=0.2$.

local matrix deformation for several capillary and Deborah numbers. Similar to the Newtonian drops in Fig. 3, the viscoelastic drop attains a "linear regime" of deformation after an initial transient. This is consistent with the observations of Mighri *et al.* (1997). Thus, the drop deformation may be analyzed in terms of the slope S as before, but now as a function of the Deborah number De.

Figure 6 shows four $S(De)$ curves for different Ca and β values. For $\beta=0.5$, two different behaviors are manifested for large and small Ca. For highly deformed drops at $Ca=2.9$, viscoelasticity promotes drop deformation. That is, the polymeric drop deforms faster than the Newtonian drop, and the difference increases monotonically with De. For moderately deformed drops at the lower $Ca=0.29$, the viscoelastic effect is non-monotonic; S first decreases with De, reaches a minimum around $De=2$ and then increases. At the largest De computed, the drop deformation is still below that of the Newtonian drop. For $\beta=0.1$, the non-monotonic behavior is seen for both Ca values.

The differing trends can be explained in terms of the "effective viscosity" of the non-Newtonian drop. The polymer stress takes a finite time ($\sim\lambda_H$) to react to flow, and as the simplest example, Fig. 7 shows the stress growth curves for a Giesekus fluid after startup of a homogeneous elongation at a constant strain rate $\dot{\epsilon}$. For short times, the polymer viscosity is smaller than its Newtonian counterpart, and indeed it decreases with De. This may be called the "weak regime" where the polymer molecules do not have time to unravel and sustain stress. For long times, the polymer stress eventually outgrows the Newtonian value, and in this "strong regime," $\bar{\eta}^+$ increases with De. The longer the polymer relaxation time, the longer the weak regime persists. Note that these so-called regimes are rather loosely defined; they refer to how $\bar{\eta}^+$ varies with De within a *certain time interval* and a *certain range of De*.

Our simulations are complicated by two additional factors. First, the flow inside the drop is not uniformly elongational but comprises regions of varying flow type and strain rate. Second, the Lagrangian unsteadiness experienced by the drop imposes a more complex deformation history than sudden startup. However, the main idea of Fig. 7 carries over: depending on how fast the polymer stress develops, the drop may have an effective

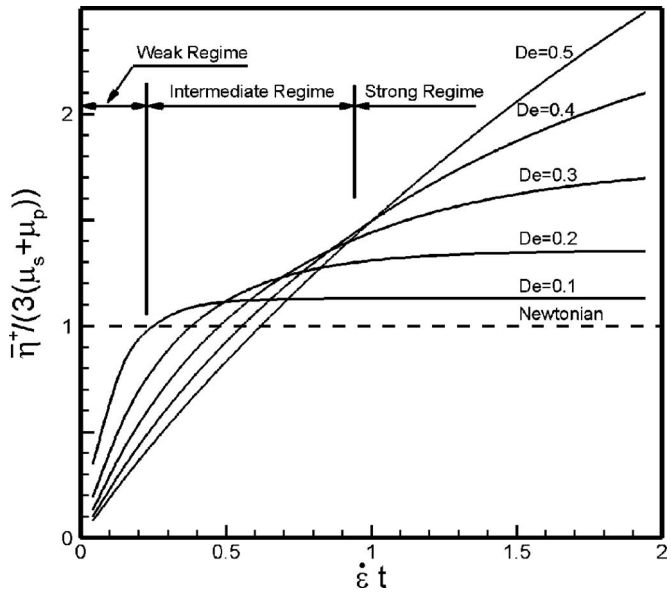

FIG. 7. Stress growth in Giesekus fluids after startup of uniaxial elongation. The elongational viscosity $\bar{\eta}^+$ is scaled by that of a Newtonian fluid with the same zero-shear viscosity $\mu_s+\mu_p$, the Deborah number is $De = \dot{\epsilon}\lambda_H$ and time is scaled by $1/\dot{\epsilon}$.

viscosity that is lower or higher than its Newtonian counterpart, which would make it deform faster or slower. In the following, we will first analyze two such scenarios for $\beta=0.5$ and $Ca=0.29$ and 2.9.

In both cases, the streamlines [top of Figs. 8(a) and 8(b)] have the same asymmetric hyperbolic pattern. However, the contours of the strain rate differ [top of Figs. 8(c) and 8(d)]. In the highly elongated drop at $Ca=2.9$, $\dot{\gamma}$ is fairly uniform inside the drop, with a weak maximum near the front tip. In the less deformed drop at $Ca=0.29$, $\dot{\gamma}$ is small in the middle of the drop but attains relatively large magnitudes near the front and the back, with a maximum at the front tip. Contours of the normal stress $N_1=\tau_{zz}-\tau_{rr}$ in the bottom halves of Figs. 8(c) and 8(d) show similar patterns.

To explain this difference, it is convenient to think of the straining inside the drop as from two possible origins: primary flow due to elongation of the drop and secondary flow (e.g., recirculating eddies) due to confinement of the interface. For a drop that deforms affinely with the matrix, the internal straining is entirely due to the first. For a drop that has attained steady shape in an elongational flow, it is entirely due to the second. As our drop stretches at a rate that is S times that of the matrix, we may take $S\boldsymbol{v}_m$ to be the primary flow inside the drop, $\boldsymbol{v}_m$ being the "background" velocity of the matrix in the absence of the drop. Then the remainder $\boldsymbol{v}-S\boldsymbol{v}_m$ represents the secondary flow. For $Ca=2.9$, the drop elongates almost affinely as $S\approx 1$ in Fig. 5(a). Thus, the flow field inside the drop is as if the interface did not exist, and the secondary flow due to the interface, plotted in the bottom of Fig. 8(a), is almost nil. For $Ca=0.29$, in contrast, the drop deforms much more slowly than the matrix [cf. Fig. 5(b)]. The secondary flow exhibits the familiar recirculating eddies in the bottom of Fig. 8(b). This pattern produces strong uniaxial extension and long residence times near the front and back stagnation points and

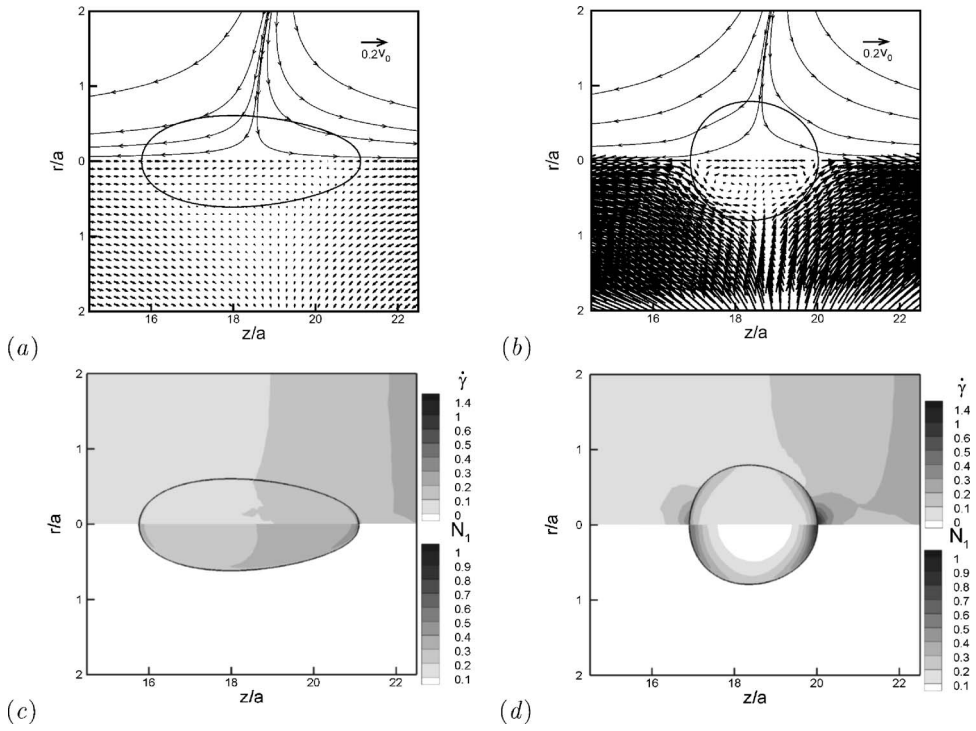

FIG. 8. Snapshots of the flow and stress fields near the Giesekus drop when D_m=2.5. β=0.5 and k=0.2. (a) Ca=2.9. The top shows streamlines in the reference frame of the drops's centroid, while the bottom plots the velocity vector field $\boldsymbol{v}-S\boldsymbol{v}_m$. (b) The same plots for Ca=0.29. The reference vector in (a) and (b) is $0.2v_0$. (c) Ca=2.9. The top and bottom respectively plot contours of the strain rate $\dot{\gamma}$ and the normal stress difference N_1. (d) The same plots for Ca=0.29.

consequently the $\dot{\gamma}$ and N_1 contours in Figs. 8(c) and 8(d), in much the same way as inside a drop that has reached steady-state deformation in steady uniaxial elongation [Ramaswamy and Leal (1999b)].

The above analysis has two implications to interpreting the viscoelastic effects on drop deformation. First, since the bulk of the drop experiences much lower stress than the maximum N_1 at the front, it is reasonable to use this maximum N_1^{max} as an indication of the drop's internal stress and hence its resistance to deformation. Second, the magnitude of $\dot{\gamma}$ in Fig. 8 possibly puts the Ca=0.29 case (with an average strain rate $\dot{\gamma}_{av}$=0.045) in the strong regime of Fig. 7 but Ca=2.9 ($\dot{\gamma}_{av}$=0.09) in the weak regime, with different dependence on the Deborah number.

This is confirmed by comparing the history of stress growth at the front tip of the drop for a range of De (Fig. 9). For Ca=0.29, the maximum stress N_1^{max} increases as De increases from 0.029 to 2.9. This is the *strong-regime* behavior, with the effective viscosity of the drop increasing with De. Referring to Fig. 4, a zero-shear viscosity ratio of β=0.5 means that we are in the range where drop deformation decreases with drop viscosity. Thus, D decreases with De in this range in Fig. 6(b). As De increases further to 14.5 and 290, the polymer stress grows more slowly, and N_1^{max} starts to decrease with De for the initial part of the drop's trajectory. This explains the subsequent increase of D with De in Fig. 6(b). The non-monotonic dependence of D on De for Ca=0.29, therefore, reflects the polymer stress inside the drop undergoing a transition from the strong to the weak regime. This is essentially the *intermediate regime* in Fig. 7 in which the elonga-

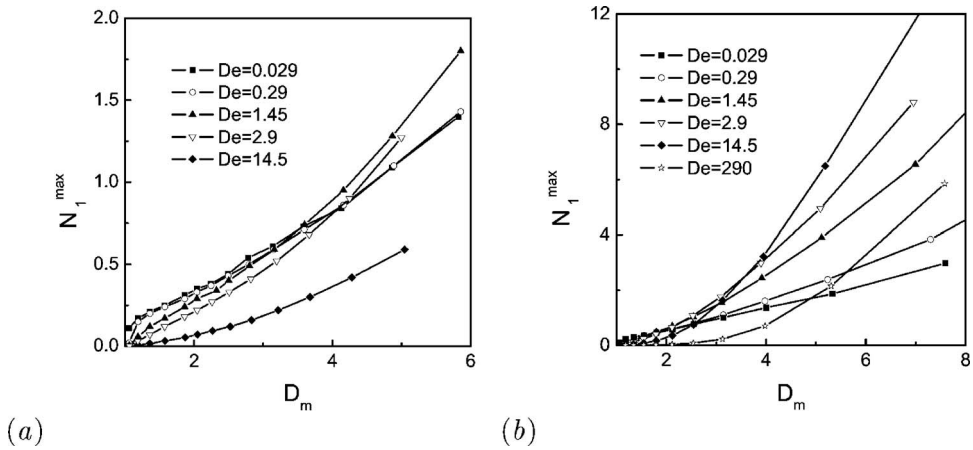

FIG. 9. History of stress growth at the front tip of the Giesekus drop for a range of *De*. (a) $Ca=2.9$; (b) $Ca=0.29$. For all curves $\beta=0.5$ and $k=0.2$.

tional viscosity at a fixed time first increases with *De* and then declines. In contrast, the polymer stress for $Ca=2.9$ remains mostly in the weak regime because the strain rate $\dot{\gamma}$ is lower in the drop and the stress grows more slowly. This is evident in Fig. 9(a) and explains the monotonic increase of *D* with *De* in Fig. 6(a).

We have performed the same analysis on the two curves in Fig. 6 for $\beta=0.1$. The quantitative difference is that $\dot{\gamma}$ inside the drop is now higher. This is easy to understand since with decreasing drop viscosity, the interfacial mobility increases. The larger $\dot{\gamma}$ amounts to shifting the dimensionless time in Fig. 7 to the right, thereby the weak regime for $\beta=0.5$ to the intermediate regime for $\beta=0.1$ in Fig. 6(a). Conceivably, the drop will still exhibit entirely weak behavior (*S* increasing monotonically with *De*) at sufficiently large *Ca*.

To summarize, the viscoelastic effect on drop deformation is rooted in the polymer stress in the drop, but manifested through a sort of "spatial integration" over extensional and rotational regions inside the drop as well as a "temporal integration" over the Lagrangian-unsteady trajectory of the drop. As in the simple picture of Fig. 7, here the polymer stress grows according to the polymer relaxation time and the local strain rate. Thus one may be tempted to relate the polymer stress to a local Deborah number. But we did not attempt to identify the local instantaneous $\dot{\gamma}$ and *De* to force a quantitative connection with the weak and strong regimes in Fig. 7. This is because the spatial and temporal variations make it impossible to define an effective *De* for the entire drop and pinpoint the time for the transition from the weak to the intermediate regime. The connection between Figs. 7 and 6 is more subtle than can be thus quantified.

C. A Newtonian drop in a Giesekus matrix

Deformation of Newtonian drops in a Giesekus matrix also displays the linear growth with matrix deformation after an initial transient, similar to the inverse case of the last subsection (Fig. 3). This is again in agreement with the experimental observations of Mighri *et al.* (1997). Thus, we continue to use the slope *S* of the growth curve as a yardstick to measure the effect of matrix viscoelasticity on drop deformation. Figure 10 plots the variation of *S* with the Deborah number *De* for two capillary numbers and two viscosity ratios. For $\beta=0.5$, drop deformation is seen to decrease monotonically with *De*

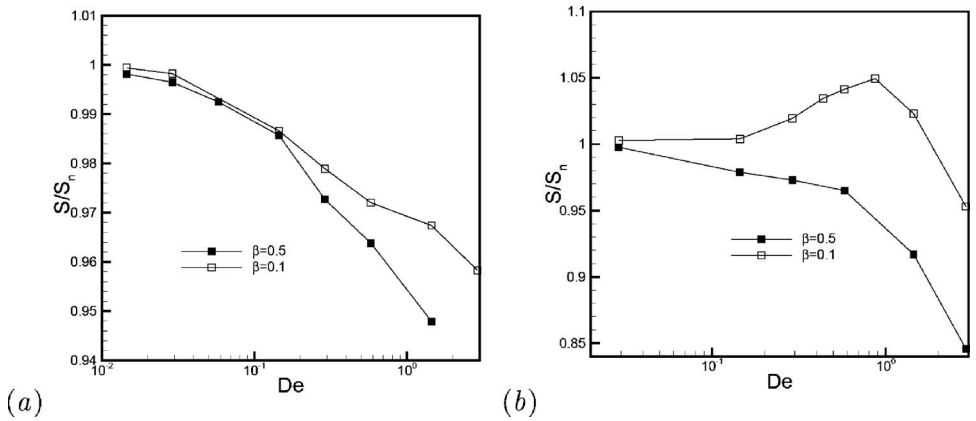

FIG. 10. Viscoelastic effects on the deformation of a Newtonian drop in a Giesekus matrix at (a) $Ca=2.9$, (b) $Ca=0.29$. The drop deformation is represented by the slope S scaled by the corresponding Newtonian slope S_n. For all cases, $k=0.7$.

for both Ca. For $\beta=0.1$, however, two different behaviors may appear. For $Ca=0.29$, S first increases with De, peaks around $De=0.9$ and then decreases for higher De to values below the Newtonian deformation. For $Ca=2.9$, S declines monotonically with increasing De.

The two trends can be explained in terms of the transient polymer stress in a similar fashion to the last subsection. A minor complication is that in the Newtonian curves of Fig. 3, Ca is defined using the matrix viscosity μ_m. While changing the drop viscosity μ_d only affects β, changing μ_m would change the capillary number as well, and the resultant change in D or S cannot be read directly off Fig. 4. If we define a capillary number Ca^* using μ_d, then the effect of changing μ_m (and thus β) with Ca^* fixed is very simple: the drop deformation decreases with β for all values of Ca^* tested. An example is shown in Fig. 11 for $Ca^*=0.029$. There is no longer the interplay between initial transient and final steady state seen in Fig. 3. Based on Fig. 11, the effect of matrix viscoelasticity can be easily interpreted through the idea that the growing polymer stress amounts to a changing effective viscosity for the matrix.

We will first explain the differing trends seen for $\beta=0.1$. The flow and stress fields near the drop, plotted in Fig. 12, show a certain similarity to those in the last subsection. Our focus, of course, now falls on the Giesekus matrix fluid surrounding the drop. Note that for the less deformed drop at $Ca=0.29$, $\dot{\gamma}$ and N_1 are much larger than the drop at $Ca=2.9$, and their maxima occur just outside the front tip of the drop. Therefore, the drop at $Ca=0.29$ may experience the *strong regime* while the latter the *weak regime*. This is borne out by the stress growth curves for a range of De at each Ca (Fig. 13). For $Ca=2.9$, the polymer stress decreases monotonically with De, showing weak regime behavior. For $Ca=0.29$, on the other hand, N_1 increases with De until $De=0.87$, and then declines with greater De. There is a transition from the strong regime for smaller De to the weak regime for larger ones. If the polymer stress amounts to, in an average sense, an effective viscosity of the viscoelastic matrix, then in view of Fig. 11, we can rationalize the monotonic decrease of S with D in Fig. 10(a) and the non-monotonic variation in Fig. 10(b).

For $\beta=0.5$, the strain rates and polymer stresses are both lower, since the higher drop

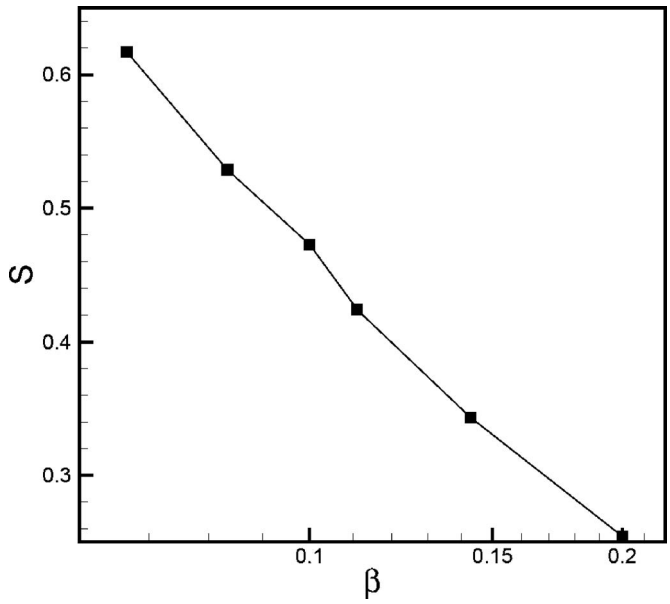

FIG. 11. The slope S as a function of the viscosity ratio β for a Newtonian drop in a Newtonian matrix with the capillary number based on the drop viscosity fixed at $Ca^*=0.029$.

viscosity reduces the interfacial mobility. Qualitatively this corresponds to shifting the dimensionless time in Fig. 7 to smaller times. Consequently the weak regime prevails for both Ca values. We omit a detailed analysis for brevity.

Based on the analysis of the last two subsections, the commonality between Figs. 6 and 10 becomes apparent. No matter whether the viscoelasticity occurs in the drop or the matrix, its effect on drop deformation may fall in the weak regime or the intermediate regime (i.e., the transition from the strong to the weak regime). The key determinant is the magnitude of $\dot{\gamma}$ inside the viscoelastic component relative to the externally imposed strain rate. A smaller Ca or β causes a higher $\dot{\gamma}$ and favors the strong regime. Generally, we may expect the De range corresponding to the strong regime to widen for decreasing Ca and/or β, and to narrow and even disappear for increasing Ca and/or β.

V. COMPARISON WITH PRIOR STUDIES

The results reported in the last section may seem inconsistent with the conventional thinking that the polymer in the drop reduces its deformation while polymer in the matrix increases deformation. That notion is based on the heuristic argument that the *steady-state* drop shape is the result of a balance among the hydrodynamic forces inside and outside the drop and the interfacial tension [Ghodgaonkar and Sundararaj (1996)]. In steady uniform elongational flows, the predictions are indeed confirmed by experiments and calculations [Ramaswamy and Leal (1999a,1999b); Tretheway and Leal (2001); Hooper *et al.* (2001b)]. The converging flow geometry produces a continuously increasing strain rate along the centerline, which keeps the polymer stress, be it in the drop or the matrix, in a perpetual transient. As a result, the drop deformation exhibits a more varied behavior than in steady elongational flow.

The experiment of Mighri *et al.* (1997) and the computation of Khayat (1998) provide the most comprehensive data in the literature on drop deformation in a conical flow

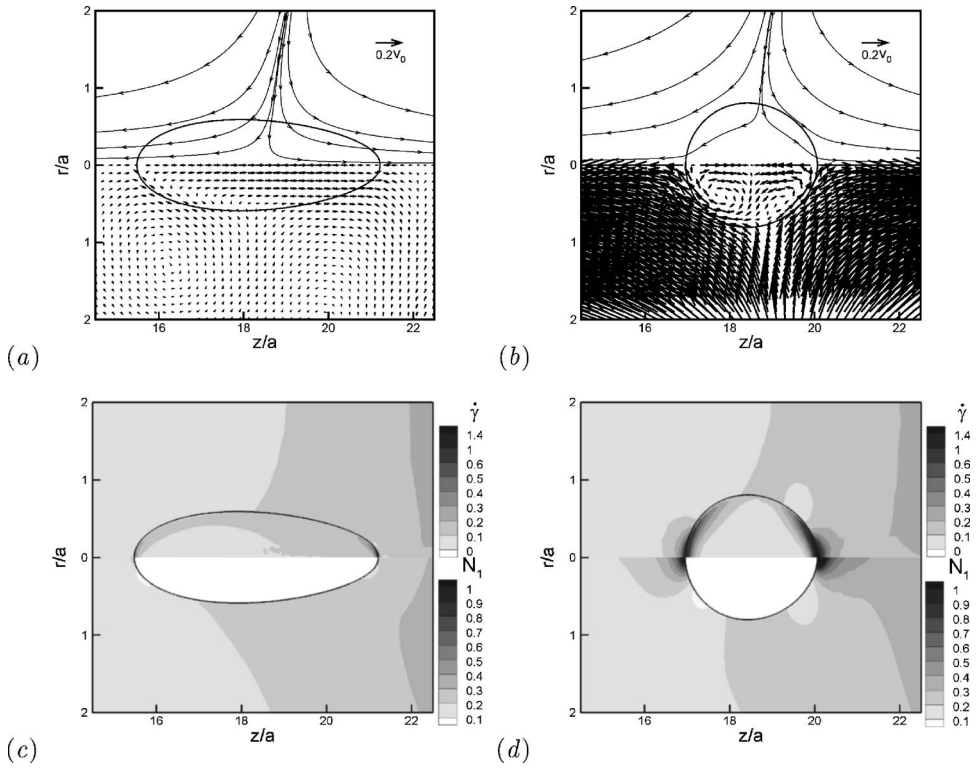

FIG. 12. Flow and stress fields near a Newtonian drop in a Giesekus matrix at D_m=2.5. β=0.1, k=0.7. The streamlines, velocity vectors and contours for $\dot{\gamma}$ and N_1 are plotted in the same way as in Fig. 8. Ca=2.9 for (a) and (c) and Ca=0.29 for (b) and (d). The reference vector in (a) and (b) is for the velocity vector plots.

geometry. Mighri *et al.* (1997) reported a linear relationship between drop deformation D and matrix deformation D_m for all Newtonian and Boger-fluid drops and matrices tested. Our predictions are consistent with these findings except that the linearity becomes es-

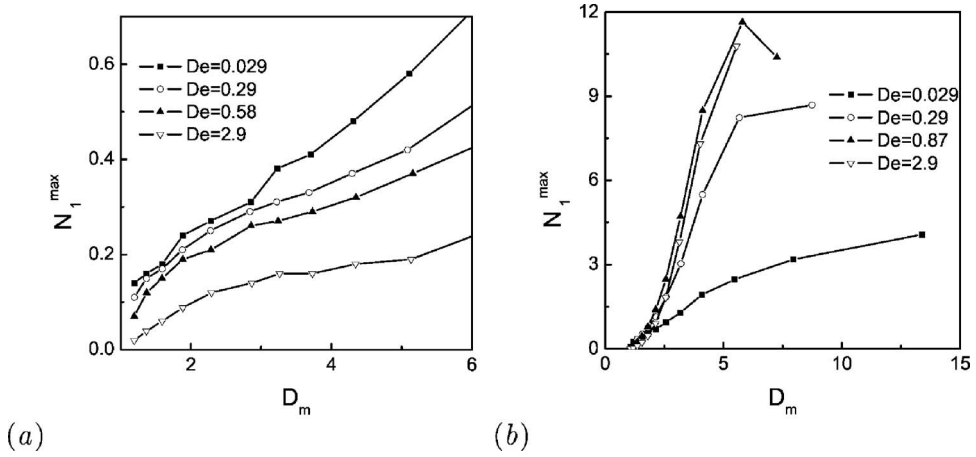

FIG. 13. History of stress growth outside the front tip of the Newtonian drop in the Giesekus matrix for a range of De. (a) Ca=2.9; (b) Ca=0.29. β=0.1 and k=0.7 for all curves.

tablished only after the influence of the initial condition dies out in the numerical simulations. For all their experimental runs, Mighri *et al.* found that viscoelasticity in the drop decreases drop deformation while that in the matrix increases it. These correspond to our strong-regime behavior. In contrast, Khayat's simulations, based on a linear Oldroyd-B model, predict purely weak-regime behavior; the drop deformation increases monotonically with De if the polymer is in the drop but decreases monotonically if in the matrix. The contradiction between these two studies can be reconciled by examining the flow and material parameters.

Using the material and experimental parameters of the experiment of Mighri *et al.*, we have determined the range of dimensionless groups as defined here: $9\times10^{-3}\leq Ca\leq 9\times10^{-2}$, $0.28\leq\beta\leq 1.1$ and $4\times10^{-3}\leq De\leq 0.14$. Comparing these parameters with Figs. 6 and 10, it is reasonable to assume that the small Ca and small De have put all the experiments within the strong regime. Khayat (1998) did not report the matrix viscosity used in his computations. If we take $\mu_m\sim 50$ Pa s from the experiment of Bourry *et al.* (1999), which Khayat (1998) aimed to simulate, then Khayat's Ca is estimated to be around 800. The viscosity ratio is also relatively large: $\beta=3$, and the Deborah number De ranges from 0.016 to 0.16. The large Ca and β imply that his simulations are well within the weak regime. Therefore, the experiment of Mighri *et al.* and Khayat's simulation fall on opposite ends of the parametric spectrum; the former is entirely in the strong regime while the latter is in the weak regime.

The strong-regime behavior is more familiar because most prior experiments have measured *steady-state* drop deformation. The only exception may be the experiment of Delaby *et al.* (1995), in which deformation of polymer inclusions in a polymer matrix is measured following startup of stretching. They reported that the drop deforms more (or less) than in a comparable Newtonian/Newtonian system if its relaxation time is longer (or shorter) than that of the matrix polymer. This trend corresponds to our weak regime. The authors invoked the linear viscoelastic theory of Palierne to explain the observations, even though the total strain is on the order of 5. A quantitative comparison with our calculations is difficult because the experiment employed uniform elongation. A further complication arises from the use of polymer melts, whose stretching may implicate both deformation-dependent viscosity and elasticity, and it is impossible to separate the two. Additional hints of weak-regime behavior come from the computational results of Hooper *et al.* (2001a). In startup of uniaxial elongation at a fixed strain rate, viscoelasticity in the drop causes a faster initial drop deformation than a Newtonian drop of the same viscosity, and a Newtonian drop deforms more slowly in a viscoelastic matrix.

To verify the weak-regime drop deformation predicted here, experiments should be designed to have low strain rates but fast transients in the Lagrange sense, with polymers of long relaxation times. This way, the polymer stress is kept in an "undeveloped stage," far from equilibrating with the local instantaneous strain rate. In the past, the strong-regime picture was long held for shear flows as well [Elmendorp and Maalcke (1985); Mighri *et al.* (1998)], until the careful low-strain-rate measurements of Guido *et al.* (2003) suggested the existence of weak-regime deformation for small De. Computational confirmation came afterwards [Yue *et al.* (2005c)]. In inhomogeneous elongational flows, our predictions of weak- and intermediate-regime drop deformation await similar experiments.

Finally, the idea of comparing the polymer relaxation time λ_H and the emulsion time t_{em} has proved useful in analyzing certain viscoelastic interfacial flows [Olbricht and Leal (1983); Grillet *et al.* (1999)]. For instance, Grillet *et al.* (1999) found the so-called elasticity parameter De/Ca an important determinant of interfacial instability in coating flows involving a viscoelastic liquid. The idea does not apply to our problem, however. A

long t_{em} implies a long transient in drop deformation, and a long λ_H indicates slow growth of polymer stress. Both conspire, rather than compete, in bringing about weak-regime behavior.

VI. CONCLUSION

In this study, we have investigated the influence of viscoelasticity on drop deformation in converging pipe flows in a conical geometry. Three series of simulations have been carried out, with Newtonian drops in a Newtonian matrix, Giesekus drops in a Newtonian matrix and Newtonian drops in a Giesekus matrix. Viscoelastic effect on drop deformation turns out to be rather subtle, and may enhance or suppress drop deformation depending on the flow and material parameters.

With the viscoelastic component in the drop or the matrix, the dependence of drop deformation on the Deborah number may be either monotonic or non-monotonic. The former is attributable to the initial weak regime in the development of the polymer stress upon startup of elongation, where the instantaneous elongational viscosity is lower for larger De. The latter corresponds to a transition from a strong regime to the weak regime, with the instantaneous stress first increasing with De and then declining. In the weak regime, a polymer drop deforms more readily than a comparable Newtonian one, and a polymer matrix is less able to deform a drop than a Newtonian matrix of the same viscosity. In the strong regime, the trend is reversed. Which behavior prevails in a conical flow channel depends on the capillary number Ca, the viscosity ratio β as well as the range of the Deborah number De. A smaller Ca and a smaller β are conducive to larger local strain rates and hence faster polymer growth, whereas a larger Ca or β favors the weak regime.

This scheme reconciles contradictory results in the literature as opposite limits in the parameter space. Thus, it provides a more or less complete picture for viscoelastic effects on drop deformation in transient elongational flows. To verify this picture experimentally, carefully designed experiments should explore low strain rates and fast transients.

ACKNOWLEDGMENTS

This work was supported by the NSERC, the Canada Research Chair Program and the Canada Foundation for Innovation. D.Z. acknowledges partial support by a University Graduate Fellowship from UBC. The manuscript was completed during a visit by J.J.F. at Shanghai Jiao Tong University, and he thanks Professor Chixing Zhou and Professor Wei Yu for their hospitality.

References

Anderson, D. M., G. B. McFadden, and A. A. Wheeler, "Diffuse-interface methods in fluid mechanics," Annu. Rev. Fluid Mech. **30**, 139–165 (1998).

Bird, R. B., R. C. Armstrong, and O. Hassager, *Dynamics of Polymeric Liquids, Vol. 1. Fluid Mechanics* (Wiley, New York, 1987a).

Bird, R. B., C. F. Curtiss, R. C. Armstrong, and O. Hassager, *Dynamics of Polymeric Liquids, Vol. 2. Kinetic Theory* (Wiley, New York, 1987b).

Bourry, D., R. E. Khayat, L. A. Utracki, F. Goudbille, J. Picot, and A. Luciani, "Extensional flow of polymeric dispersions," Polym. Eng. Sci. **39**, 1072–1086 (1999).

Chin, H. B., and C. D. Han, "Studies on droplet deformation and breakup. I. Droplet deformation in extensional flow," J. Rheol. **23**, 557–590 (1979).

Cogswell, F. N., "Measuring the extensional rheology of polymer melts," J. Rheol. **16**, 383–403 (1972).

Delaby, I., B. Ernst, Y. Germain, and R. Muller, "Droplet deformation in polymer blends during uniaxial elongational flow: Influence of viscosity ratio for large capillary numbers," J. Rheol. **38**, 1705–1720 (1994).

Delaby, I., R. Muller, and B. Ernst, "Drop deformation during elongational flow in blends of viscoelastic fluids. Small deformation theory and comparison with experimental results," Rheol. Acta **34**, 525–533 (1995).

Elmendorp, J. J., and R. J. Maalcke, "A study on polymer blending microrheology: Part I," Polym. Eng. Sci. **25**, 1041–1047 (1985).

Feng, J. J., C. Liu, J. Shen, and P. Yue, "An energetic variational formulation with phase field methods for interfacial dynamics of complex fluids: Advantages and challenges," in *Modeling of Soft Matter*, edited by M.-C. T. Calderer, and E. Terentjev (Springer, New York, 2005), pp. 1–26.

Ghodgaonkar, P. G., and U. Sundararaj, "Prediction of dispersed phase drop diameter in polymer blends: The effect of elasticity," Polym. Eng. Sci. **36**, 1656–1665 (1996).

Greco, F., "Drop deformation for non-Newtonian fluids in slow flows," J. Non-Newtonian Fluid Mech. **107**, 111–131 (2002).

Grillet, A. M., A. G. Lee, and E. S. G. Shaqfeh, "Observations of ribbing instabilities in elastic fluid flows with gravity stabilization," J. Fluid Mech. **399**, 49–83 (1999).

Guido, S., M. Simeone, and F. Greco, "Deformation of a Newtonian drop in a viscoelastic matrix under steady shear flow. Experimental validation of slow flow theory," J. Non-Newtonian Fluid Mech. **114**, 65–82 (2003).

Hooper, R., M. Toose, C. W. Macosko, and J. J. Derby, "A comparison of boundary element and finite element methods for modeling axisymmetric polymeric drop deformation," Int. J. Numer. Methods Fluids **37**, 837–864 (2001a).

Hooper, R. W., V. F. de Almeida, C. W. Macosko, and J. J. Derby, "Transient polymeric drop extension and retraction in uniaxial extensional flows," J. Non-Newtonian Fluid Mech. **98**, 141–168 (2001b).

Jacqmin, D., "Calculation of two-phase Navier-Stokes flows using phase-field modeling," J. Comput. Phys. **155**, 96–127 (1999).

Khan, S. A., and R. G. Larson, "Comparison of simple constitutive equations for polymer melts in shear and biaxial and uniaxial extensions," Eng. Anal. Boundary Elem. **31**, 207–234 (1987).

Khayat, R. E., "Boundary element analysis of planar drop deformation in confined flow. Part II. Viscoelastic fluids," Eng. Anal. Boundary Elem. **22**, 291–306 (1998).

Khismatullin, D., Y. Renardy, and M. Renardy, "Development and implementation of VOF-PROST for 3D viscoelastic liquid-liquid simulations," J. Non-Newtonian Fluid Mech. **140**, 120–131 (2006).

Kim, S. J., and C. D. Han, "Finite element analysis of axisymmetric creeping motion of a deformable non-Newtonian drop in the entrance region of a cylindrical tube," J. Rheol. **45**, 1279–1303 (2001).

Liu, C., and J. Shen, "A phase field model for the mixture of two incompressible fluids and its approximation by a Fourier-spectral method," Physica D **179**, 211–228 (2003).

Lowengrub, J., and L. Truskinovsky, "Quasi-incompressible Cahn-Hilliard fluids and topological transitions," Proc. R. Soc. London, Ser. A **454**, 2617–2654 (1998).

Mighri, F., A. Ajji, and P. J. Carreau, "Influence of elastic properties on drop deformation in elongational flow," J. Rheol. **41**, 1183–1201 (1997).

Mighri, F., P. J. Carreau, and A. Ajji, "Influence of elastic properties on drop deformation and breakup in shear flow," J. Rheol. **42**, 1477–1490 (1998).

Olbricht, W. L., and L. G. Leal, "The creeping motion of immiscible drops through a converging/diverging tube," J. Fluid Mech. **134**, 329–355 (1983).

Rallison, J. M., "The deformation of small viscous drops and bubbles in shear flows," Annu. Rev. Fluid Mech. **16**, 45–66 (1984).

Ramaswamy, S., and L. G. Leal, "The deformation of a Newtonian drop in the uniaxial extensional flow of a viscoelastic liquid," J. Non-Newtonian Fluid Mech. **88**, 149–172 (1999a).

Ramaswamy, S., and L. G. Leal, "The deformation of a viscoelastic drop subjected to steady uniaxial extensional flow of a Newtonian fluid," J. Non-Newtonian Fluid Mech. **85**, 127–163 (1999b).

Sethian, J. A., and P. Smereka, "Level set methods for fluid interfaces," Annu. Rev. Fluid Mech. **35**, 341–372 (2003).

Sibillo, V., M. Simeone, and S. Guido, "Break-up of a Newtonian drop in a viscoelastic matrix under simple shear flow," Rheol. Acta **43**, 449–456 (2004).

Sibillo, V., M. Simeone, S. Guido, F. Greco, and P. Maffettone, "Start-up and retraction dynamics of a Newtonian drop in a viscoelastic matrix under simple shear flow," J. Non-Newtonian Fluid Mech. **134**, 27–32 (2006).

Stone, H. A., "Dynamics of drop deformation and breakup in viscous fluids," Annu. Rev. Fluid Mech. **26**, 65–102 (1994).

Stone, H. A., B. J. Bentley, and L. G. Leal, "An experimental study of transient effects in the breakup of viscous drop," J. Fluid Mech. **173**, 131–158 (1986).

Tirtaatmadja, V., and T. Sridhar, "Comparison of constitutive equations for polymer solutions in uniaxial extension," J. Rheol. **39**, 1133–1160 (1995).

Tretheway, D. C., and L. G. Leal, "Deformation and relaxation of Newtonian drops in planar extensional flows of a Boger fluid," J. Non-Newtonian Fluid Mech. **99**, 81–108 (2001).

Tucker, C. L., and P. Moldenaers, "Microstructural evolution in polymer blends," Annu. Rev. Fluid Mech. **34**, 177–210 (2002).

van der Reijden-Stolk, C., and A. Sara, "A study on polymer blending microrheology. Part 3. Deformation of Newtonian drops submerged in another Newtonian fluid flowing through a converging cone," Polym. Eng. Sci. **26**, 1229–1239 (1986).

Yue, P., J. J. Feng, C. Liu, and J. Shen, "Diffuse-interface simulations of drop coalescence and retraction in viscoelastic fluids," J. Non-Newtonian Fluid Mech. **129**, 163–176 (2005a).

Yue, P., J. J. Feng, C. Liu, and J. Shen, "Transient drop deformation upon startup of shear in viscoelastic fluids," Phys. Fluids **17**, 123101 (2005b).

Yue, P., J. J. Feng, C. Liu, and J. Shen, "Viscoelastic effects on drop deformation in steady shear," J. Fluid Mech. **540**, 427–437 (2005c).

Yue, P., C. Zhou, and J. J. Feng, "A computational study of the coalescence between a drop and an interface in Newtonian and viscoelastic fluids," Phys. Fluids **18**, 102102 (2006a).

Yue, P., C. Zhou, and J. J. Feng, "Spontaneous shrinkage of drops and mass conservation in phase-field simulations," J. Comput. Phys. **223**, 1–9 (2007).

Yue, P., C. Zhou, J. J. Feng, C. F. Ollivier-Gooch, and H. H. Hu, "Phase-field simulations of interfacial dynamics in viscoelastic fluids using finite elements with adaptive meshing," J. Comput. Phys. **219**, 47–67 (2006b).

Zhou, C., P. Yue, and J. J. Feng, "Simulation of neutrophil deformation and transport in capillaries using simple and compound drop models," Ann. Biomed. Eng. **35**, 766–780 (2007).